Earth and Planetary Science Letters 478 (2017) 76–88

Contents lists available at ScienceDirect

Earth and Planetary Science Letters

www.elsevier.com/locate/epsl

Rapid fore-arc extension and detachment-mode spreading following subduction initiation

Antony Morris [a,*], Mark W. Anderson [a], Ahmed Omer [a,1], Marco Maffione [b], Douwe J.J. van Hinsbergen [c]

[a] School of Geography, Earth and Environmental Sciences, University of Plymouth, Drake Circus, Plymouth PL4 8AA, UK
[b] School of Geography, Earth and Environmental Sciences, University of Birmingham, Edgbaston, Birmingham B15 2TT, UK
[c] Department of Earth Sciences, University of Utrecht, Utrecht, Netherlands

ARTICLE INFO

Article history:
Received 24 May 2017
Received in revised form 15 August 2017
Accepted 24 August 2017
Available online 15 September 2017
Editor: J. Brodholt

Keywords:
ophiolite
paleomagnetism
subduction initiation
suprasubduction zone
fore-arc extension
metamorphic sole

ABSTRACT

Most ophiolites have geochemical signatures that indicate formation by suprasubduction seafloor spreading above newly initiated subduction zones, and hence they record fore-arc processes operating following subduction initiation. They are frequently underlain by a metamorphic sole formed at the top of the downgoing plate and accreted below the overlying suprasubduction zone lithosphere immediately following ophiolite formation. Paleomagnetic analyses of ophiolites can provide important insights into the enigmatic geodynamic processes operating in this setting via identification of tectonic rotations related to upper plate extension. Here we present net tectonic rotation results from the Late Cretaceous Mersin ophiolite of southern Turkey that document rapid and progressive rotation of ophiolitic rocks and their associated metamorphic sole. Specifically, we demonstrate that lower crustal cumulate rocks and early dykes intruded into the underlying mantle section have undergone extreme rotation around ridge-parallel, shallowly-plunging axes, consistent with oceanic detachment faulting during spreading. Importantly, later dykes cutting the metamorphic sole experienced rotation around the same axis but with a lower magnitude. We show that these rotations occurred via a common mechanism in a pre-obduction, fore-arc setting, and are best explained by combining (hyper)extension resulting from detachment-mode, amagmatic suprasubduction zone spreading in a fore-arc environment with a recently proposed mechanism for exhumation of metamorphic soles driven by upper plate extension. Available age constraints demonstrate that extreme rotation of these units was accommodated rapidly by these processes over a time period of $<\sim 3$ Myr, comparable with rates of rotation seen in oceanic core complexes in the modern oceans.

1. Introduction

Ophiolites provide insights into fundamental oceanic tectonic processes associated with their formation at spreading axes and subsequent intraoceanic- and emplacement-related deformation. The majority of the world's ophiolites have a geochemical signature interpreted as indicating formation above newly initiated intraoceanic subduction zones, in so-called suprasubduction zone environments (e.g. Pearce and Robinson, 2010). This setting can also account for the observation that ophiolite accretion is often closely followed by subduction-related emplacement onto continental margins (Robertson, 2002). In contrast to true mid-ocean ridge systems, suprasubduction zone ophiolite formation and subsequent evolution is the result of a complex process controlled by both the subducting plate and tectonic processes in the fore-arc region. This is clearly demonstrated by the occurrence of so-called metamorphic soles below many suprasubduction zone ophiolites. Metamorphic soles are thin (<500 m) layers of granulite to greenschist facies rocks, which experienced high temperature and pressure metamorphism (850–900 °C, 10–15 kbar) above a subducting lithosphere, prior to their accretion to the overriding plate (for a review see van Hinsbergen et al., 2015). In several well-preserved ophiolites like that of Oman, the metamorphic sole is spread over a broad area below the ophiolite, up to c. 100 km away from the paleo-trench, suggesting original accretion as a large semi-continuous metamorphic layer. The accretion of metamorphic soles below ophiolites necessarily requires some sort of fore-arc thinning to exhume the sole from peak metamorphic depths, either tectonically via extension of the overriding plate (e.g.

* Corresponding author.
E-mail address: amorris@plymouth.ac.uk (A. Morris).
[1] Permanent address: Technical Institute of Kirkuk, Kirkuk, Republic of Iraq.

http://dx.doi.org/10.1016/j.epsl.2017.08.040
0012-821X/

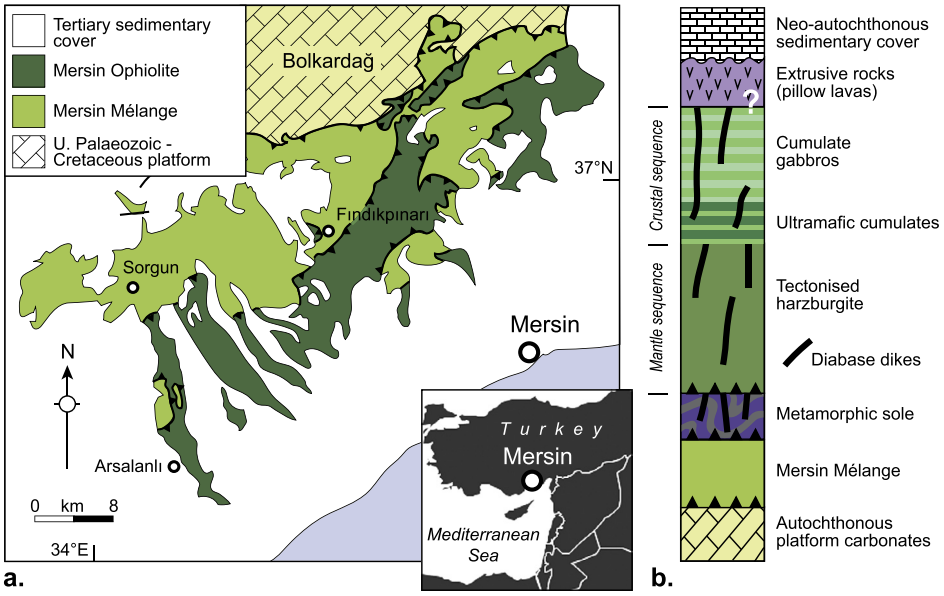

Fig. 1. Summary of the geology of the Mersin ophiolite of southern Turkey. (a) Simplified geological map (after Tekin et al., 2016); (b) tectonostratigraphic column (after Parlak et al., 1996b). In this study we have sampled dykes cutting the metamorphic sole of the ophiolite, dykes cutting the mantle sequence, and ultramafic and gabbroic cumulates of the lower crust for paleomagnetic analysis. (A color version of this figure is available with the web version of the article.)

Hacker and Gnos, 1997), or magmatically via partial melting and resulting volume decrease of the forearc mantle wedge below the newly formed suprasubduction zone crust (van Hinsbergen et al., 2015). The similarity of ages of ophiolitic crust and peak metamorphism of associated metamorphic soles observed in nearly all ophiolites indicates that spreading and metamorphic sole exhumation are almost simultaneous processes, and both occur during or shortly after subduction initiation.

Obtaining geological evidence that constrains the kinematics and timing of tectonic processes affecting fore-arc systems during subduction initiation in the modern oceans is difficult as incipient subduction zones are rare (Gurnis et al., 2004). Hence, well-exposed ophiolites provide important records of fore-arc processes operating during and following subduction initiation that are otherwise difficult to investigate (Stern and Bloomer, 1992; Robertson, 2002). Numerous studies have highlighted how paleomagnetic analyses of ophiolites can help to unravel the tectonic evolution of these systems. A focus has been the Tethyan ophiolites of the eastern Mediterranean/Middle East region, where magnetic techniques have been used to constrain the structure and orientation of suprasubduction spreading axes (e.g. Allerton and Vine, 1987; Hurst et al., 1992; Morris and Maffione, 2016; Maffione et al., 2017), patterns of magmatic flow during crustal accretion (e.g. Staudigel et al., 1992; Granot et al., 2011), the kinematics of transform fault systems (e.g. Morris et al., 1990; MacLeod et al., 1990; Morris and Maffione, 2016), and the response of the upper plate to impingement of continental margins with subduction zones (Clube et al., 1985; Inwood et al., 2009; Morris et al., 2002).

Renewed interest in ophiolites has followed the discovery of the importance of oceanic detachment faulting and the formation of oceanic core complexes (OCCs) in slow-ultraslow spreading lithosphere in the Atlantic and Indian Oceans (e.g. Smith et al., 2008; MacLeod et al., 2017) and the definition of a new amagmatic "detachment-mode" of seafloor spreading (Escartín and Canales, 2011). This is fundamentally different from classic magmatic spreading and involves plate divergence being taken up by slip on lithospheric-scale faults that rotate during displacement, resulting in exhumation of their footwall sections and exposure of lower crustal and mantle rocks on the seafloor. Studies of samples recovered by scientific ocean drilling have shown 45–65° rolling-hinge rotations of OCC footwalls in the Atlantic Ocean around ridge-parallel, sub-horizontal axes (Garcés and Gee, 2007; Morris et al., 2009; MacLeod et al., 2011). This characteristic has allowed Maffione et al. (2013) to extend the record of detachment-mode spreading back to the Jurassic by demonstrating the existence of a fossil OCC preserved within the Mirdita ophiolite of Albania. More recently, Maffione et al. (2015) showed that oceanic detachment faulting was responsible for large tectonic rotations and extensional thinning of fore-arc lithosphere preserved in the Cretaceous ophiolites of southern Tibet. This led them to propose a new concept of "fore-arc hyperextension", demonstrating how the exchange of ideas between studies in the modern oceans and in ophiolites can lead to advances in our understanding of lithospheric processes.

Here we present the first paleomagnetic data from the Late Cretaceous Mersin ophiolite of southern Turkey. Like many Tauride ophiolites (Dilek et al., 1999), Mersin consists predominantly of tectonized mantle rocks and ultramafic/mafic cumulates, with no sheeted dyke complex and only limited exposures of extrusive rocks, and is underlain by a metamorphic sole that has ^{40}Ar–^{39}Ar cooling ages that are similar to the age of the ophiolitic magmatic rocks (Parlak et al., 2013; van Hinsbergen et al., 2016). Our data constrain the axes, magnitudes and timing of tectonic rotations in these units, and provide evidence for rapid fore-arc (hyper)extension via detachment-mode seafloor spreading (Escartín and Canales, 2011). We show that this style of Neotethyan suprasubduction zone spreading provides a viable mechanism to explain the exhumation of metamorphic soles, their structural disruption following welding to the base of the lithosphere, and the lack of upper crustal sequences in many Tauride ophiolites.

2. The Mersin ophiolite

The Mersin ophiolite complex outcrops over a 60 km long, 25 km wide area in southern Turkey (Fig. 1a). It consists of an Upper Cretaceous ophiolite sequence, underlain by metamorphic sole rocks and then by the Mersin Mélange (Fig. 1b; Parlak and Delaloye, 1996, 1999; Parlak et al., 2013). These units form the highest structural unit of the uppermost Cretaceous–Eocene Tau-

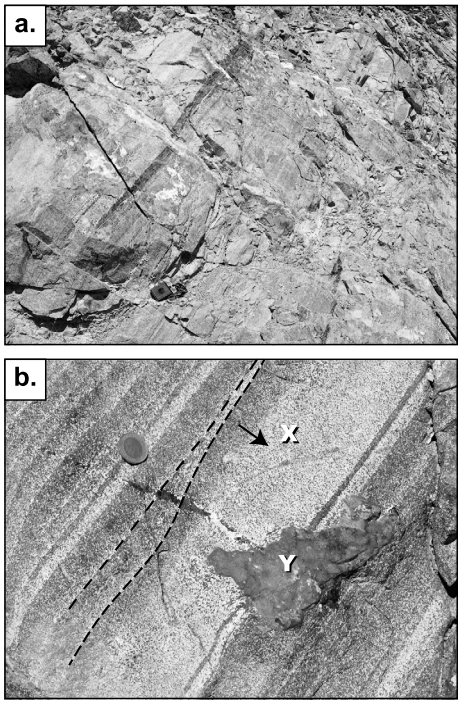

Fig. 2. (a) Modal compositional layering in cumulate gabbros exposed along the Sorgun valley in the Mersin ophiolite (site MC09; compass-clinometer for scale). (b) Close-up of modal layering (coin for scale). In this example, compositional grading from olivine-rich bases to plagioclase-rich tops (X) combined with scour structures (dashed lines) provide way-up indicators that indicate overturning of the section. Darker area (Y) is a remnant of a thin (<3 cm thick) basaltic dyke cutting the gabbros (sampled as site MC10).

ride fold-thrust belt dominated by Paleozoic–Mesozoic platform carbonates (Robertson, 2002).

The ophiolite has a suprasubduction zone geochemical signature (Parlak et al., 1996a) and consists of tectonized peridotites (harzburgites and dunites), ultramafic and mafic cumulates, isotropic gabbro, minor plagiogranites, and rare basalts associated with deep marine sediments (Parlak et al., 1996a). The cumulate rocks are best exposed along the Sorgun valley (between the villages of Sorgun and Arsalanlı; Fig. 1a), where ~800 m of ultramafic cumulates at the base pass upwards into ~2500 m of modally layered gabbroic rocks consisting of gabbro, olivine gabbro and anorthosite (Parlak et al., 1996a). Way-up criteria (mineralogical grading; evidence of scouring at the base of some layers; Fig. 2) indicate that steeply-dipping modal compositional layering in the gabbros is in places overturned. The cumulate layers are occasionally intruded at a high angle by thin, fine-grained basaltic dykes.

Lower levels of the ophiolite are best exposed in the Fındıkpınarı valley area (Fig. 1a), nearly 20 km to the NE of the Sorgun valley, providing sections through both the mantle sequence and the metamorphic sole. The latter has a thickness of about 50–70 m and consists predominantly of amphibolites, amphibolitic schists, epidote-amphibolite schists, quartz-mica schists, calcschists and marble, with a typical inverted metamorphic zonation from upper amphibolite at the top to greenschist facies at the bottom (Parlak et al., 1996b). The sole rocks are intensely deformed, with development of a pronounced foliation, a NW–SE-trending mineral stretching lineation and intrafolial folds (Parlak et al., 1996b). Kinematic indicators all indicate a top to the NW shear sense during formation of the sole (Parlak et al., 1996b).

Both the tectonized harzburgite and sole are cut by undeformed, discrete doleritic dykes composed of plagioclase, clinopyroxene and amphibole, with subophitic and microgranular textures and variable degrees of hydrothermal alteration. They have geochemical signatures similar to evolved island-arc tholeiites and were derived from a mantle wedge that underwent previous melt extraction and subsequent metasomatism by LILE- and light REE-enriched fluids (Dilek et al., 1999). Dykes hosted by tectonized harzburgite are up to 5 m thick and dip at ~30° to the ~ESE, whereas those hosted by the metamorphic sole are characteristically thinner (<1 m), clearly post-metamorphic and post-shearing, and dip at ~55° to the ~NW.

Available high precision ^{40}Ar–^{39}Ar and U–Pb age constraints for the Mersin ophiolite and its metamorphic sole are summarized in Table 1. Only one U–Pb zircon date is available from the Mersin gabbros (Parlak et al., 2013), yielding an age of 82.8 ± 4.0 Ma. This Is deemed unreliable, however, due to evidence for hydrothermal alteration of the dated zircons, and the age of crystallization of the suprasubduction zone crust regionally is considered by Parlak et al. (2013) to be ~89 Ma. The remaining data indicate that intrusion of dykes into the mantle sequence, formation of the metamorphic sole (cooling through amphibolite facies conditions) and intrusion of dykes through the sole were broadly synchronous events. This has important implications for the rapidity of the rotations determined from the paleomagnetic data presented here.

3. Sampling and methods

To quantify tectonic rotations that have affected the Mersin ophiolite, we sampled the lower crustal sequence (ultramafic and gabbroic cumulates) exposed continuously along the Sorgun valley section (Fig. 1a), together with dolerite dykes cutting tectonized harzburgites of the mantle sequence, and dolerite dykes cutting the metamorphic sole of the ophiolite (both exposed near the village of Fındıkpınarı; Fig. 1a). An average of eight samples per site were drilled *in situ* using standard paleomagnetic procedures, yielding up to 13 specimens per site for analysis. Sampling was restricted to exposures that showed either consistent planar layering in cumulate rocks or dykes with parallel planar margins. Structural orientations were measured in the field to an accuracy of ± 5°.

Natural remanences were measured in the University of Plymouth palaeomagnetic laboratory using either Molspin or AGICO JR-6A fluxgate spinner magnetometers (with respective noise levels of 0.05×10^{-3} and 0.01×10^{-3} A/m). Specimens were subjected to either alternating field (AF) demagnetization using an AGICO LDA-3A demagnetizer in 13 incremental steps from 5 to 100 mT or thermal demagnetization using a Magnetic Measurements MMTD80A demagnetizer with 19 temperature increments from 100 to 580 °C (or until complete demagnetization). Demagnetization data were displayed on orthogonal vector plots and remanence components isolated via principal component analysis using MacPaleomag software (written by Jeff Gee, Scripps Institution of Oceanography). Site mean directions were evaluated using Fisherian statistics on virtual geomagnetic poles (VGPs) corresponding to the isolated characteristic remanent magnetizations (ChRMs). Paleomagnetic quality criteria proposed by Deenen et al. (2011) were adopted to estimate the reliability of the ChRM/VGP distribution at the site level. In particular, the VGP scatter (i.e., A_{95}) obtained at each site was compared to the expected scatter induced by paleosecular variation (PSV) of the geomagnetic field (i.e., A_{95min}–A_{95max}) to assess whether PSV was sufficiently represented in our datasets (Deenen et al., 2011). For values of $A_{95} < A_{95min}$ PSV is not adequately represented, indicating insufficient time averaging of the geomagnetic field (i.e. resulting from rapid cooling), slow cooling and protracted acquisition of remanence (such that PSV is largely averaged at the specimen level) or remagnetization. Conversely, values of $A_{95} > A_{95max}$ may indicate additional (tectonic) processes responsible for an enhanced scatter of paleomagnetic directions. Site mean magnetization directions were interpreted using a net tectonic rotation approach

Table 1
Summary of geochronological constraints from the Mersin ophiolite.

Rock	Mineral/whole rock	Method	Age (Ma)	Error	Sample code	Reference
Gabbro	Zircon	U-Pb	82.8	4.0	FK57	Parlak et al. (2013)
Dolerite dyke in mantle	Hornblende	$^{40}Ar/^{39}Ar$	91.0	0.6	MO-92-3	Dilek et al. (1999)
Amphibolite	Hornblende	$^{40}Ar/^{39}Ar$	91.0	0.8	93-MO-5	Dilek et al. (1999)
Amphibolite	Hornblende	$^{40}Ar/^{39}Ar$	91.3	0.4	93-MO-22	Dilek et al. (1999)
Amphibolite	Hornblende	$^{40}Ar/^{39}Ar$	93.7	0.3	OP 257	Parlak and Delaloye (1999)
Amphibolite	Hornblende	$^{40}Ar/^{39}Ar$	96.1	0.3	OP 256	Parlak and Delaloye (1999)
Amphibolite	Hornblende	$^{40}Ar/^{39}Ar$	93.6	0.4	OP 255	Parlak and Delaloye (1999)
Amphibolite	Hornblende	$^{40}Ar/^{39}Ar$	93.9	0.4	OP 254	Parlak and Delaloye (1999)
Amphibolite	Hornblende	$^{40}Ar/^{39}Ar$	91.8	0.3	OP 253	Parlak and Delaloye (1999)
Amphibolite	Hornblende	$^{40}Ar/^{39}Ar$	92.7	0.3	OP 132	Parlak and Delaloye (1999)
Amphibolite	Hornblende	$^{40}Ar/^{39}Ar$	91.9	0.3	OP 131	Parlak and Delaloye (1999)
		Mean:	92.9	1.6 (1σ)		
Dolerite dyke in sole	Whole rock	$^{40}Ar/^{39}Ar$	89.8	0.3	OP 122	Parlak and Delaloye (1996)
Dolerite dyke in sole	Whole rock	$^{40}Ar/^{39}Ar$	89.5	0.4	OP 129	Parlak and Delaloye (1996)

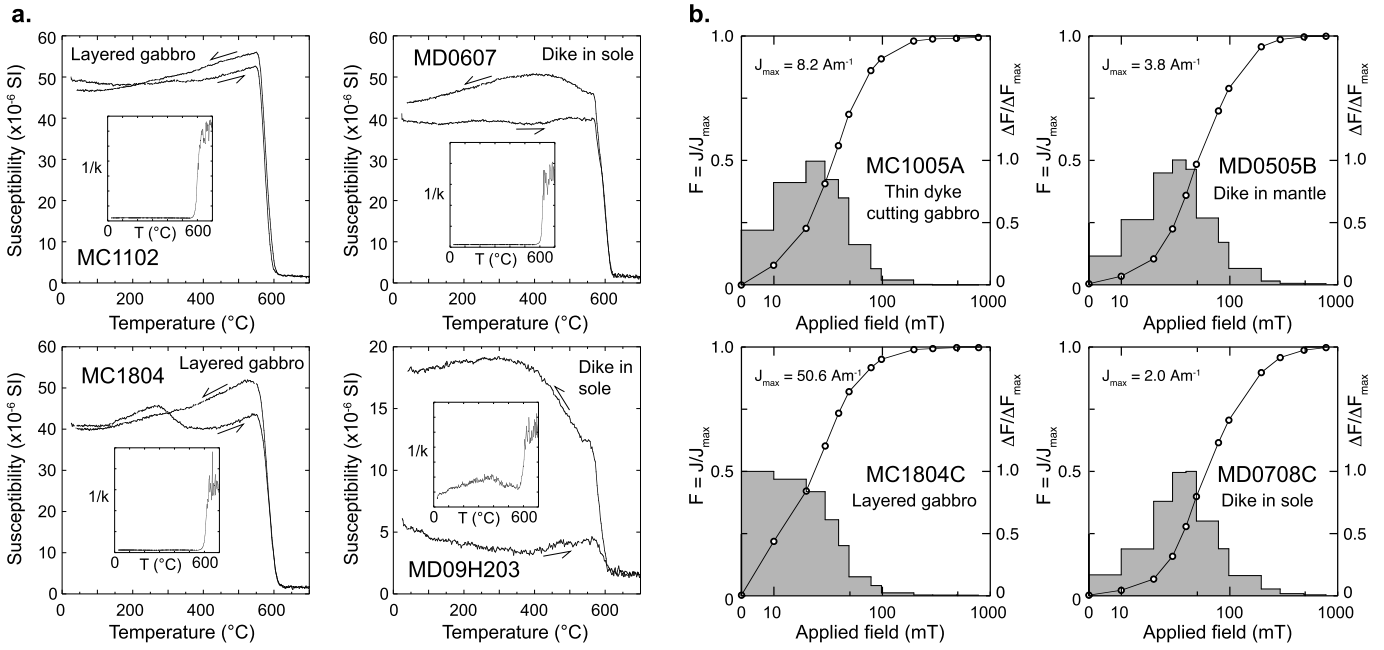

Fig. 3. (a) High-temperature variations of low-field magnetic susceptibility (k) showing maximum Curie temperatures of ~580 °C. Inset diagrams show the variation of $1/k$, allowing accurate determination of Curie temperatures using the Petrovský and Kapička (2006) method. (b) Isothermal remanent magnetization (IRM) acquisition curves showing presence of low coercivity magnetite.

(Allerton and Vine, 1987; Morris et al., 1998) to determine rotation axes and magnitudes and recover the initial strikes of dykes. This technique is discussed more fully below.

Rock magnetic experiments were performed to characterize remanence-carrying minerals in sampled lithologies. The high-temperature (20–700 °C) variation of magnetic susceptibility, k, of representative samples was measured in an argon atmosphere using an AGICO Kappabridge KLY-3S coupled with a CS-3 furnace. Curie temperatures were determined from these experiments by the Petrovský and Kapička (2006) method on $1/k$ data using the AGICO program Cureval v. 8.0.2. Isothermal remanent magnetization (IRM) acquisition experiments were conducted on representative samples to determine coercivity spectra (using a Molspin pulse magnetizer to apply peak fields up to 800 mT, with resulting IRMs measured using an AGICO JR-6A spinner magnetometer), followed by backfield IRM experiments to determine coercivities of remanence. Ferromagnetic phases were further characterized in thin section by optical microscopy and by EDX spectral analyses performed on a JEOL7001 FEG-SEM and analyzed using Oxford Instruments Aztec software.

4. Results and analysis

4.1. Magnetic mineralogy and palaeomagnetic results from the ophiolite

High-temperature variation of magnetic susceptibility experiments revealed consistent maximum Curie temperatures of ~580 °C (Fig. 3a), indicating that the ferromagnetic fraction in both cumulate rocks and dykes includes near-stoichiometric magnetite. Some specimens exhibit increased susceptibility upon cooling, suggesting production of new magnetite during heating. A limited number of specimens (e.g. specimen MC1804 in Fig. 3a) show a hump in the heating curve between 150–400 °C. The increasing temperature limbs of these humps are reversible until 300 °C, but become irreversible after further heating, suggesting the presence of titanomagnetite/titanomaghemite in addition to magnetite. IRM acquisition experiments show that saturation is reached at applied fields of 200–300 mT (Fig. 3b) indicating presence of low coercivity minerals in these rocks. Backfield IRM experiments yield coercivity of remanence values of 24–53 mT suggesting presence of fine-grained single domain or pseudo-single domain magnetite. These

rock magnetic observations are consistent with petrographic and SEM analyses that show that magnetite and minor titanomagnetite are the dominant oxides present in both cumulate rocks and dykes. In the ultramafic cumulates (sites MC01-03), secondary magnetite is present in serpentinized olivine grains, whereas primary magnetite (plus titanomagnetite) with little alteration is observed in the cumulate gabbros and diabase dykes. Ferromagnetic pyrrhotite is also occasionally seen in the dykes, but demonstrably carries the same magnetization direction as the dominant magnetite phase. Overall, these results are entirely compatible with those obtained in other Late Cretaceous Neotethyan ophiolites in this region (e.g. Troodos, Hatay, Baër-Bassit, Alihoca, Göksun, Divriği; Morris et al., 1998, 2002; Inwood et al., 2009; Morris and Maffione, 2016; Maffione et al., 2017), where magnetic remanences have been shown to be of primary, pre-deformational origin, acquired during or shortly after seafloor spreading.

Intensities of natural remanences in these rocks vary by lithology, with highest average intensities in the layered gabbros (1.12 A/m) and lower values of 132 mA/m and 80 mA/m in the ultramafic cumulates and dykes, respectively. Stable components of magnetization were isolated at all sites, following removal of occasional minor secondary components during initial demagnetization. Typical examples of demagnetization behavior are shown in Fig. 4. Most samples are dominated by univectorial, single component decay to the origin. Both AF and thermal demagnetization experiments yielded identical remanence directions (Fig. 4). Stable components of magnetization were identified from individual specimens and subsequently combined to give a mean ChRM for each site. These *in situ* magnetic remanences are given in Table 2 and shown with corresponding specimen directions and VGPs in the stereographic equal area projections of Supplemental Fig. 1. With the exception of one specimen (at site MD11), all VGPs fell within the 45° cut-off at each site recommended by Johnson et al. (2008). Directions are unrelated to the present-day geocentric axial dipole field in the Mersin region ($D = 000°$, $I = 56°$), excluding recent remagnetization. Cumulate rocks (ultramafic cumulates and layered gabbros) have NE-directed *in situ* ChRMs with negative inclinations, indicating substantial tectonic rotation since magnetization acquisition. Dykes hosted in the mantle sequence also have *in situ* negative inclinations, whereas those cutting the metamorphic sole have shallow positive inclinations, with both sets having generally northerly declinations.

VGP scatter at 11 out of 28 sites (Table 2) is within the limits of that expected from PSV (Deenen et al., 2011), consistent with a primary origin of the remanence. Underrepresentation of PSV at remaining sites is interpreted to reflect significant averaging of secular variation at the sample level during slow cooling of the cumulate rocks (as seen in samples of lower crustal gabbros recovered by scientific ocean drilling; Gee and Kent, 2007) and of dykes intruded into the mantle sequence and metamorphic sole.

4.2. Reference direction

Remanence directions must be compared to an appropriate reference direction to determine the extent of tectonic rotation affecting the ophiolite. In our analysis, the reference direction has a declination = 000°, assuming an original normal magnetic polarity as the ophiolite formed during the Cretaceous Normal Superchron (C34N). This implies that calculated net rotations arise from a combination of plate motion and intra-plate deformation. The inclination of the reference direction was determined from paleolatitude estimates based on kinematic reconstructions (van Hinsbergen et al., 2016) placed in the paleomagnetic reference frame of Torsvik et al. (2012). Uncertainties in the reference inclination relate to the reconstructed width of the Neotethys Ocean and the A_{95} error of the reference global apparent polar wander path. Reconstructions for the Late Cretaceous at 100–90 Ma constrain the Neotethyan spreading axis to lie between the southern margin of Eurasia at 33 ± 3°N and the northern margin of Gondwana at 16 ± 3°N. We have no other paleolatitudinal control on the position of the future Mersin ophiolite within these limits, and therefore used a paleolatitude of 24.5 ± 11.5°N to encompass this range. Assuming a geocentric axial dipole field, this corresponds to a reference inclination of 40.2 ± 15.4°.

4.3. Determination of net tectonic rotations

Standard paleomagnetic structural corrections involve untilting inferred paleohorizontal/vertical surfaces around strike-parallel axes. Corrected declinations are then compared to the reference direction to determine vertical axis rotations. This approach therefore arbitrarily decomposes the total deformation at a site into rotations around two orthogonal axes (vertical and horizontal). Interpretations then frequently focus entirely on the vertical axis rotations, ignoring the tilting component of the deformation. In complexly deformed terrains, where fold axes are seldom horizontal and where multiple phases of deformation may occur, this procedure can introduce serious declination errors (MacDonald, 1980). It is more appropriate, therefore, to describe the deformation at a site in terms of a single rotation about an inclined axis, which restores both the paleosurface to its initial orientation and the site mean magnetization vector to the reference direction. This single rotation may then be decomposed into any number of component rotations on the basis of additional structural data. Importantly, in the case of dykes, this approach can resolve rotations around margin-normal axes that are impossible to observe in the field and that act as a source of error when standard tilt corrections are employed (Morris and Anderson, 2002). This approach also facilitates back-stripping of later rotations from the total deformation to recover earlier rotations.

Here we use the net tectonic rotation method of Allerton and Vine (1987), which has been employed effectively in numerous previous studies in ophiolites (e.g., Morris et al., 1990, 1998, 2002; Hurst et al., 1992; Inwood et al., 2009; Maffione et al., 2015, 2017; Morris and Maffione, 2016; van Hinsbergen et al., 2016). This technique (Supplemental Fig. 2) can be applied to either paleovertical or paleohorizontal cases, with the key assumption that no internal deformation of a sampled unit has occurred. In this case, the angle β between the site magnetization vector (SMV) and the present day pole to the paleosurface (PDP) remains constant during deformation (Allerton and Vine, 1987). A circle of radius β centred on the reference magnetization vector (RMV) therefore defines the locus of potential positions of the initial pole to the paleosurface. In the case of a dyke, the intersections of this circle with the horizontal represent the poles to two possible vertical initial dyke orientations (Supplemental Fig. 2), and additional constraints are required to select a preferred solution. If a vertical solution cannot be found then the dyke initial strike is invariable and fixed by the reference direction and we exclude the result from the analysis of restored dyke trends. In the case of cumulate rocks, an initial pole for the paleosurface is selected at the steepest point on the circle of radius β centred on the RMV in order to restore the structure to a minimum possible dip (Supplemental Fig. 2). In all cases, the SMV is then restored to the RMV and the PDP to its initial orientation by rotating around an axis at the intersection of the planes (great circles) bisecting the pairs of vectors (Supplemental Fig. 2). The net tectonic rotation is described by the azimuth and plunge of this rotation axis and the angle and sense of rotation.

In a modification of this method used here (Morris et al., 1998; Koymans et al., 2016), the effects of uncertainties on the input vectors are modeled by applying the Allerton and Vine (1987) algorithm to all combinations of three estimates of the reference

Table 2
Paleomagnetic results from the Mersin ophiolite. Orientation of paleosurfaces (dyke margins; cumulate layering) are expressed as dip direction/dip. O/T = overturned. D, I, declination and inclination of *in situ* site mean remanence. ΔD, ΔI, declination and inclination error, respectively. k, α_{95}, precision parameter and 95% cone of confidence around the site mean characteristic remanent magnetizations (ChRMs). K, A_{95}, precision parameter and 95% cone of confidence around the site mean virtual geomagnetic pole (VGP). A_{95min}, A_{95max}, minimum and maximum value of A_{95} expected from paleosecular variation of the geomagnetic field, according to Deenen et al. (2011). N, number of total samples used for the statistics.

Site	Description	Latitude (°N)	Longitude (°E)	Orientation	Mean remanence vector				k	α_{95}	K	A_{95}	A_{95min}	A_{95max}	N
					D	ΔD	I	ΔI							
Metamorphic sole-hosted dikes:															
MD06	Diabase dike	36°53′31.75″	34°20′01.53″	307/38	6.7	5.0	11.3	9.7	42.0	6.8	76.7	5.0	4.4	17.1	12
MD07	Diabase dike	36°53′32.63″	34°20′01.10″	328/64	10.5	2.0	16.8	3.8	311.6	2.5	460.9	2.0	4.4	17.1	12
MD08	Diabase dike	36°53′33.35″	34°20′00.79″	330/50	1.8	4.2	11.5	8.0	80.2	4.9	111.1	4.1	4.4	17.1	12
MD09	Diabase dike	36°53′34.02″	34°20′01.00″	322/66	8.3	3.1	29.2	4.8	147.5	3.8	242.5	2.9	4.6	18.1	11
Mantle-hosted dikes:															
MD01	Diabase dike	36°53′41.31″	34°21′39.39″	160/70	331.1	9.2	34.0	13.3	31.0	8.3	28.5	8.7	4.6	18.1	11
MD02	Diabase dike	36°53′37.86″	34°21′37.47″	185/44	3.7	13.0	−73.3	4.1	130.4	3.8	43.6	6.7	4.4	17.1	12
MD03	Diabase dike	36°53′36.79″	34°21′37.33″	104/28	24.0	3.4	−55.3	2.7	308.4	2.5	253.9	2.7	4.4	17.1	12
MD04	Diabase dike	36°53′36.40″	34°21′37.52″	108/24	17.1	5.4	−64.0	3.0	269.3	2.6	134.9	3.8	4.4	17.1	12
MD05	Diabase dike	36°53′34.53″	34°21′39.71″	152/40	35.6	3.6	−48.4	3.6	243.2	2.8	193.2	3.1	4.4	17.1	12
MD10	Diabase dike	36°53′19.67″	34°20′19.42″	144/75	353.3	5.3	−0.8	10.5	35.7	7.0	63.3	5.3	4.3	16.3	13
MD11	Diabase dike	36°53′11.32″	34°20′51.59″	081/44	15.2	3.7	−50.0	3.6	244.2	2.8	187.7	3.2	4.4	17.1	12
Crustal section:															
MC01	Ultramafic cumulates	36°48′42.15″	34°10′14.01″	177/69	49.1	7.1	−22.1	12.4	32.1	10.8	76.7	6.9	5.5	24.1	7
MC02	Ultramafic cumulates	36°48′40.45″	34°10′11.81″	175/67	42.8	3.3	0.9	6.7	121.4	4.4	210.9	3.3	4.8	19.2	10
MC03	Ultramafic cumulates	36°48′34.52″	34°10′11.19″	136/59	40.9	8.4	−19.4	15.3	25.6	11.2	45.3	8.3	5.2	22.1	8
MC04	Layered gabbro	36°48′27.14″	34°10′35.78″	352/82 O/T	61.8	4.7	−34.7	6.7	87.3	4.7	97.7	4.4	4.4	17.1	12
MC05	Layered gabbro	36°48′25.46″	34°10′38.05″	332/50 O/T	54.8	6.5	−32.6	9.6	43.9	6.6	50.8	6.1	4.4	17.1	12
MC06	Layered gabbro	36°48′21.26″	34°10′58.93″	332/63 O/T	64.8	3.1	−25.0	5.2	189.0	3.5	260.2	3.0	4.8	19.2	10
MC07	Layered gabbro	36°48′20.48″	34°10′59.12″	350/70 O/T	63.5	2.7	−36.7	3.7	243.0	2.7	264	2.6	4.3	16.3	13
MC08	Layered gabbro	36°48′13.16″	34°11′03.85″	318/60 O/T	63.0	2.8	−21.9	4.8	207.9	3.2	285.8	2.7	4.6	18.1	11
MC09	Layered gabbro	36°48′09.27″	34°11′03.55″	318/60 O/T	60.9	4.9	−25.5	8.2	69.2	5.3	84.2	4.8	4.4	17.1	12
MC10	Thin basaltic dike cutting MC09 gabbros	36°48′09.01″	34°11′04.35″	183/52	54.8	4.4	−25.6	7.3	65.7	5.2	95.5	4.3	4.3	16.3	13
MC11	Layered gabbro	36°48′08.60″	34°11′05.60″	318/60 O/T	52.3	3.3	−26.2	5.4	191.5	3.1	189.2	3.2	4.4	17.1	12
MC12	Layered gabbro	36°48′08.30″	34°11′06.96″	320/68 O/T	61.8	3.1	−25.0	5.2	177.4	3.3	209.5	3.0	4.4	17.1	12
MC13	Layered gabbro	36°48′07.93″	34°11′10.91″	177/87	75.9	2.4	−22.5	4.2	308.8	2.5	340.3	2.4	4.4	17.1	12
MC14	Layered gabbro	36°48′04.74″	34°11′15.38″	185/64	38.0	3.9	−33.3	5.8	105.5	4.2	137.6	3.7	4.4	17.1	12
MC16	Layered gabbro	36°45′34.11″	34°11′50.00″	006/82 O/T	67.8	5.3	−43.1	6.2	97.8	4.4	83.8	4.8	4.4	17.1	12
MC17	Layered gabbro	36°45′22.06″	34°11′55.10″	160/62	11.3	4.0	−7.7	8.0	78.6	5.2	128.9	4.0	4.6	18.1	11
MC18	Layered gabbro	36°45′19.28″	34°11′53.56″	132/52	48.1	2.9	−13.7	5.4	208.5	3.6	329.9	2.8	5.0	20.5	9

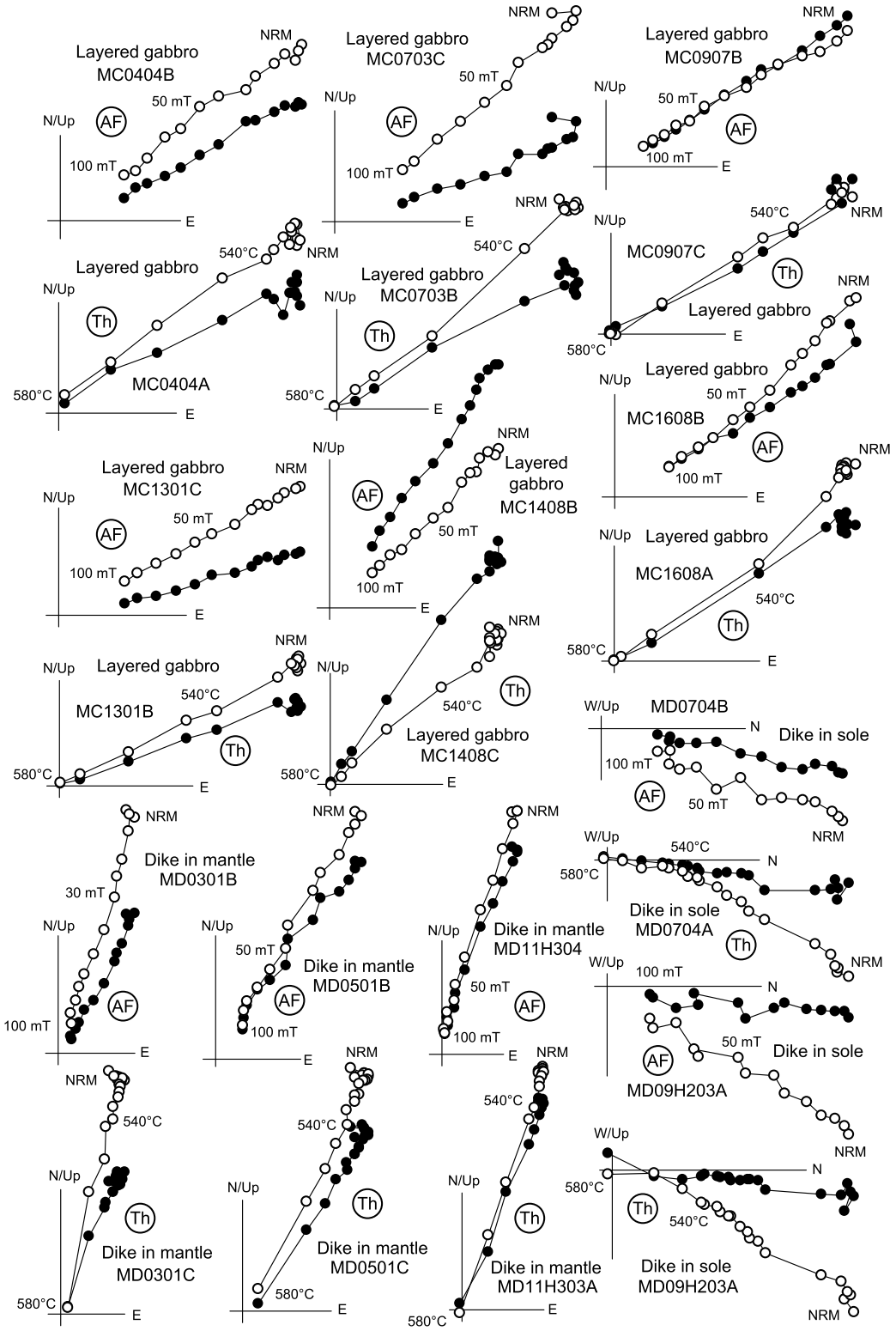

Fig. 4. Typical examples of orthogonal demagnetization diagrams, showing well-defined, characteristic remanence directions isolated by both alternating field (AF) and thermal (Th) treatment in all lithologies. Solid circles = horizontal plane; open symbols = vertical N–S or E–W plane.

inclination (mean plus two values at the edge of its error bar), and five estimates each of the SMV and present day pole to paleosurface (see Supplemental Fig. 2). This yields 75 estimates of the rotation parameters at each site, defining a non-circular distribution of acceptable rotation axes. The mean rotation axis can be determined using Bingham statistics (orientation of maximum eigenvector), and the distribution of rotation angles plotted as histograms (Supplemental Fig. 2) and described by the mean value and standard deviation. Restored dyke trends can be represented on rose diagrams, with the mean strike determined from the intermediate eigenvector of the corresponding distribution of initial dyke poles. When distributions of rotation parameters at multiple sites overlap, these may be amalgamated to determine the most robust overall solution.

Table 3
Net tectonic rotation parameters for dykes and cumulate rocks of the Mersin ophiolite.

Site	Description	N	Preferred solution					Alternative solution				
			Rotation axis		Rotation		Initial dike strike	Rotation axis		Rotation		Initial dike strike
			Azimuth	Plunge	Magnitude	Sense		Azimuth	Plunge	Magnitude	Sense	
Metamorphic sole-hosted dykes:												
MD06	Diabase dike	75	34.3	27.4	61.4	CW	12.1	352.8	23.4	114.8	CCW	347.9
MD07	Diabase dike	71	58.7	33.5	36.3	CW	44.4	353.1	23.4	100.3	CCW	315.6
MD08	Diabase dike	69	42.3	20.1	46.4	CW	43.4	343.6	23.1	90.5	CCW	316.6
MD09	Diabase dike	75	32.3	42.4	35.7	CW	29.6	358.8	32.3	110.5	CCW	330.4
	Overall mean	**290**	**39.8**	**31.3**	**45.0**	**CW**	**31.9**	**352.2**	**25.7**	**104.4**	**CCW**	**328.1**
Mantle-hosted dykes:												
MD02	Diabase dike	74	59.9	−8.9	123.3	CW	42.9	304.8	−11.1	125.2	CCW	317.1
MD03	Diabase dike	36	45.6	−3.9	116.7	CW	63.0	281.9	−13.4	88.9	CCW	297
MD04	Diabase dike	29	46.1	−10.1	116.6	CW	66.3	278.1	−8.3	92.7	CCW	293.7
MD05	Diabase dike	75	46.1	4.4	130.1	CW	32.5	308	−18.5	99.9	CCW	327.5
MD11	Diabase dike	43	30.4	−5.5	131.7	CW	60.2	262.5	−6.6	84.9	CCW	299.8
	Overall mean	**257**	**47.3**	**−3.9**	**125.0**	**CW**	**48.4**	**293**	**−13.1**	**102.3**	**CCW**	**311.6**
Cumulate rocks:												
MC01	Ultramafic cumulates	75	71.8	29.6	97.2	CW						
MC02	Ultramafic cumulates	75	53.6	39.2	92.5	CW						
MC03	Ultramafic cumulates	75	62.7	26.3	96.5	CW						
MC04	Layered gabbro	75	64.9	21.4	121.9	CW						
MC05	Layered gabbro	75	46.0	13.0	142.6	CW						
MC06	Layered gabbro	75	51.4	20.1	142.7	CW						
MC07	Layered gabbro	75	60.7	18.4	129.2	CW						
MC08	Layered gabbro	75	47.4	19.7	148.1	CW						
MC09	Layered gabbro	75	47.5	17.5	145.7	CW						
MC11	Layered gabbro	75	44.4	16.8	140.7	CW						
MC12	Layered gabbro	75	48.7	18.8	144.2	CW						
MC13	Layered gabbro	75	68.9	31.5	127.5	CW						
MC14	Layered gabbro	75	83.5	22.3	88.3	CW						
MC16	Layered gabbro	75	59.8	13.5	135.9	CW						
MC17	Layered gabbro	75	56.3	18.6	65.1	CW						
MC18	Layered gabbro	75	66.6	34.5	94.3	CW						
	Overall mean	**1200**	**58.0**	**22.9**	**119.5**	**CW**						
Mantle-hosted dykes after backstripping the preferred mean rotation of dykes in the metamorphic sole:												
MD02	Diabase dike	70	44.1	−25.7	95.1	CW	41.1	305.1	14.3	122.2	CCW	318.9
MD03	Diabase dike	36	30.5	−16.6	83.4	CW	63.1	291.5	18.7	74.8	CCW	296.9
MD04	Diabase dike	27	26.4	−23.7	87.6	CW	65.3	286.8	22.7	77.5	CCW	294.7
MD05	Diabase dike	75	34.7	−4.3	92.3	CW	32.5	313.3	11.1	98.9	CCW	327.5
MD11	Diabase dike	44	13.3	−8.9	98.3	CW	60.8	267.9	26.5	62.9	CCW	299.2
	Overall mean	**252**	**31.7**	**−15.1**	**92.4**	**CW**	**47.8**	**298.9**	**17.4**	**93.4**	**CCW**	**312.2**
Cumulate rocks after backstripping the preferred mean rotation of dykes in the metamorphic sole:												
MC01	Ultramafic cumulates	75	82.0	12.6	61.5	CW						
MC02	Ultramafic cumulates	75	67.5	35.9	51.1	CW						
MC03	Ultramafic cumulates	75	69.7	12.2	57.4	CW						
MC04	Layered gabbro	75	74.6	7.9	78.6	CW						
MC05	Layered gabbro	75	38.8	7.8	101.8	CW						
MC06	Layered gabbro	75	47.6	13.5	100.4	CW						
MC07	Layered gabbro	75	58.0	6.5	89.4	CW						
MC08	Layered gabbro	75	42.8	15.0	105.2	CW						
MC09	Layered gabbro	75	42.2	12.5	103.8	CW						
MC11	Layered gabbro	75	38.2	12.4	98.3	CW						
MC12	Layered gabbro	75	44.0	13.3	101.6	CW						
MC13	Layered gabbro	75	73.4	18.9	88.5	CW						
MC14	Layered gabbro	75	95.2	−4.7	60.0	CW						
MC16	Layered gabbro	75	54.5	2.1	97.4	CW						
MC17	Layered gabbro	75	61.8	−15.8	27.9	CW						
MC18	Layered gabbro	75	80.3	20.9	55.6	CW						
	Overall mean	**1200**	**60.1**	**11.6**	**79.9**	**CW**						

4.4. Net tectonic rotation solutions

Out of 28 sampled sites, 25 gave net tectonic rotation solutions that are considered reliable. The three rejected sites are: (i) two dyke sites (MD01 and MD10) that gave scattered rotation axes and too few vertical solutions to be considered reliable; and (ii) a thin basaltic dyke (site MC10) intruding the layered gabbros of site MC09, that has a direction of magnetization statistically indistinguishable from its host rocks and that is not considered separately in the analysis of rotations. Mean net tectonic rotation parameters at the remaining sites are given in Table 3. In the case of the dyke sites (Table 3), our preferred solutions are those with NE–SW-directed rotation axes as these: (i) are consistent with results from the cumulate section; (ii) yield more consistent rotation angles between sites than the alternative solutions; and (iii) produce initial NE–SW dyke strikes that are in agreement with a regional-scale dataset of restored Neotethyan paleo-spreading directions recently reported by Maffione et al. (2017).

Fig. 5 illustrates the distributions of rotation parameters amalgamated by lithostratigraphic level in the ophiolite, whereas results at individual sites are shown in Supplemental Fig. 3 (for dyke sites) and Supplemental Fig. 4 (for cumulate sites). The analyses demonstrate that all levels of the Mersin ophiolite have experienced significant tectonic rotation around shallowly-plunging, NE–SW-directed axes. The overall mean rotation parameters (Table 3; Fig. 5) for the three sampled lithostratigraphic levels are:

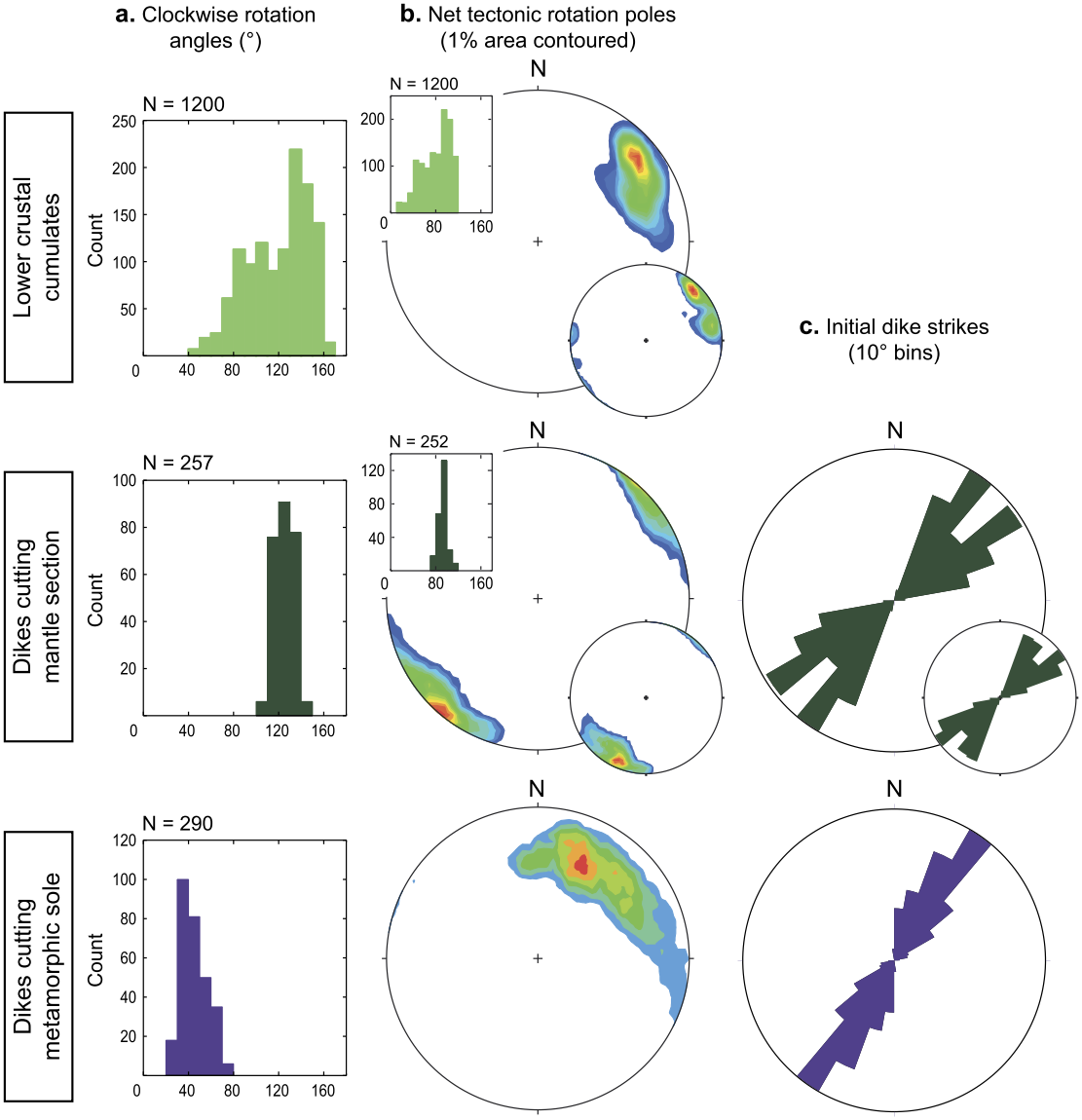

Fig. 5. Net tectonic rotation results from the Mersin ophiolite, combining site-level preferred solutions from each lithostratigraphic unit. (a) Histograms of rotation angles; (b) contoured equal area stereographic projections of rotation axes; and (c) rose diagrams of restored initial dike strikes. Note that rotation axes are consistently NE–SE-directed and parallel to initial dike strikes. Inset diagrams show the results for early rotation of the dykes cutting the mantle section and for lower crustal cumulates found by back-stripping the mean net tectonic rotation determined from dykes in the metamorphic sole (representing the latest component of rotation in the Mersin ophiolite). (A color version of this figure is available with the web version of the article.)

Cumulate section: 120.0° ± 27.4° clockwise rotation, axis = 058°/23°, $N = 1200$
Mantle-hosted dykes: 125.0° ± 8.4° clockwise rotation, axis = 047°/−04°, $N = 257$
Metamorphic sole-hosted dykes: 45.0° ± 11.8° clockwise rotation, axis = 040°/31°, $N = 290$

where errors on rotation angles are ± 1 standard deviation.

This indicates that, despite a present day geographic separation of c. 20 km, the mantle and crustal sections of the ophiolite display structural integrity and experienced a common rotation history since acquiring their magnetizations. The metamorphic sole has also experienced rotation around a similar NE–SW-directed axis but with a much lower magnitude. This is considered to represent the latest phase of rotation to affect the ophiolite and potentially reflects a combination of intraoceanic and emplacement-related deformation. We assume that this net rotation also affected the overlying mantle and crustal sites. This assumption is supported by similar initial strikes for the mantle- and metamorphic sole-hosted dykes (Fig. 5), that suggests intrusion of these units occurred in a common stress field associated with upper plate extension during formation of the ophiolite in a suprasubduction zone setting. The earlier phase of rotation affecting the mantle and crustal sections can then be determined by back-stripping the effect of the later rotation of the metamorphic sole prior to calculation of revised net tectonic rotation parameters for these units (Table 3). This yields the following mean rotation parameters:

Cumulate section 79.9° ± 25.7° clockwise rotation, axis = 060°/12°, $N = 1200$
Mantle-hosted dykes: 92.4° ± 8.2° clockwise rotation, axis = 032°/−15°, $N = 252$
Combined: 82.1° ± 24.1° clockwise rotation, axis = 056°/08°, $N = 1452$

The combined result represents the best estimate for early tilting of the sampled parts of the future ophiolite prior to emplacement of dykes into its metamorphic sole, and confirms that all phases of deformation involved rotation around similar, shallow NE-directed

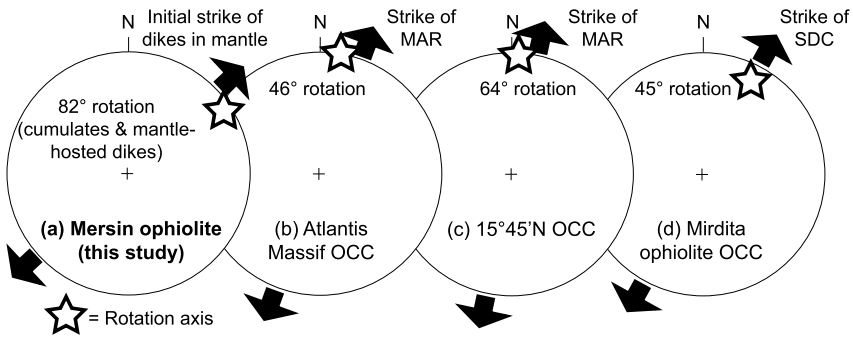

Fig. 6. Equal area stereographic projections comparing (a) the style of the early rotation of the cumulate and mantle-hosted dykes of the Mersin ophiolite with footwall rotations documented in (b) the Atlantis Massif (Morris et al., 2009) and (c) 15°45′N (MacLeod et al., 2011) OCCs on the Mid Atlantic Ridge (MAR) and in (d) a fossil OCC preserved in the Mirdita ophiolite of Albania (Maffione et al., 2013). The results for the Mersin ophiolite shown here represents an average amalgamating all net tectonic rotations solutions after back-stripping the effects of the later rotation of the metamorphic sole. Note that in all cases, rotation axes are shallowly-plunging and parallel to the observed or inferred orientation of the associated spreading axis.

axes. Moreover, given the close timing of crustal accretion, cooling of the metamorphic sole and dyke intrusion (Parlak and Delaloye, 1996, 1999; Dilek et al., 1999; Parlak et al., 2013), these data indicate that rotations accumulated progressively within the ophiolite over a very short time interval of $<\sim 3$ Myr, requiring a tectonic environment capable of generating rapid and large rotations.

5. Discussion

5.1. Tectonic environment for extreme and rapid early rotation of the Mersin ophiolite

The early phase of rotation documented above is demonstrably of intraoceanic origin and associated with suprasubduction zone spreading of the Mersin ophiolite as it occurs between two phases of dyke emplacement. In addition, rotation axes are broadly aligned with the restored trends of dykes in both the mantle sequence and metamorphic sole. Assuming that these are intruded perpendicular to the suprasubduction zone extension direction, this indicates rotation dominated by tilting around ridge-parallel axes.

In seafloor spreading systems, large rotations around shallowly plunging axes may be accommodated by normal faulting during plate divergence. For example, net tectonic rotation analyses in Troodos have highlighted rotations of dykes and lavas in the hanging wall of listric normal faults (Allerton and Vine, 1987; Hurst et al., 1992) during the development of axial and off-axis graben structures by upper crustal extension. These faults dip symmetrically towards graben axes and are inferred to flatten at depth to sole out into detachments at the base of the upper crust (at the dyke-gabbro transition; Varga and Moores, 1985), without affecting deeper levels of the ophiolite. Large listric faults that dip towards the spreading axis have also been observed by seismic imaging in the slow-spreading Atlantic Ocean (e.g. Salisbury and Keen, 1993), but these sole out near the base of the crust. To accommodate the rotations observed in the Mersin ophiolite by listric faulting during spreading would, however, require faults that sole out at the base of the lithosphere (within the upper mantle). In addition, even if lithospheric-scale listric faults were capable of accommodating rotation of the Mersin crust and upper mantle, they would be incapable of capturing rocks of the metamorphic sole at depth (i.e. near their detachment level) and rotating these as well.

In contrast to downwards-convex listric faulting, displacement on upwards-convex oceanic detachment faults (Escartín and Canales, 2011) provides a viable potential mechanism for rotation of upper mantle, crustal and metamorphic sole rocks. Investigations of oceanic core complexes in the modern oceans (Garcés and Gee, 2007; Morris et al., 2009; MacLeod et al., 2011) have shown that rolling hinge rotation of detachment fault footwalls around sub-horizontal, ridge-parallel axes is a characteristic signature of these lithospheric-scale structures. Within ophiolites, Maffione et al. (2013) showed that such fault systems may be recognized paleomagnetically using this characteristic rotation style. Most recently, Maffione et al. (2015) used a net tectonic rotation approach to document rotations around sub-horizontal axes of mantle-hosted intrusions in the Lower Cretaceous suprasubduction zone ophiolites of south Tibet. Maffione et al. (2015) suggested that these rotations result from upper plate extension accommodated by widespread detachment faulting. They termed this process “fore-arc hyperextension” and inferred that structural dismemberment occurred shortly after magmatic accretion.

We propose that the early rotation documented in the Mersin ophiolite likewise is related to fore-arc (hyper)extension taken up by detachment-mode suprasubduction zone spreading. This is supported by four lines of argument: (i) rolling hinge rotations of the footwalls of oceanic detachment faults are characterized by ridge-parallel, sub-horizontal rotation axes (Garcés and Gee, 2007; Morris et al., 2009; MacLeod et al., 2011), directly comparable to the style of rotation seen in Mersin (Fig. 6); (ii) rotation during the development of oceanic core complexes occurs very rapidly, as required by the full Mersin dataset based upon available age constraints. For example, along the Mid Atlantic Ridge, 46° of rotation of the Atlantis Massif footwall occurred in $<$1.2 Myr (Morris et al., 2009), whereas 64° of rotation of the 15°45′N oceanic complex was achieved within a very narrow inferred period of activity spanning a time interval between $\sim$2.5 to 2.1 Ma (MacLeod et al., 2011); (iii) oceanic detachment faults are lithospheric-scale structures that in the modern oceans have demonstrably exhumed mantle rocks onto the seafloor (Cannat et al., 2006), and are therefore capable of rotating both crustal and mantle sections of the Mersin ophiolite around the same axis, in contrast to “standard” oceanic normal faults that only affect the brittle upper crust; and (iv) displacement on oceanic detachment faults tectonically juxtaposes rotated lower crustal and upper mantle rocks in their footwalls with unrotated upper crustal lavas in hanging wall blocks (MacLeod et al., 2009), providing a plausible explanation for similar geological relationships in the Mersin and other Tauride ophiolites (where limited exposures of extrusive rocks are in close proximity to lower crustal/upper mantle rocks without an intervening sheeted dyke complex).

We note that the c. 82° early rotation seen in the Mersin ophiolite exceeds the range of footwall rotations observed in single oceanic detachment fault systems such as those sampled in the Atlantic Ocean (Fig. 6). However, numerical modeling of detachment faulting at slow-spreading ridges (Tucholke et al., 2008) suggests that the active root zone of a weak, asymmetric fault should mi-

grate with its hanging wall across the axis of rifting if magmatic accretion in the hanging wall takes up <<50% of the plate separation (Tucholke et al., 2008; MacLeod et al., 2009; Supplemental Fig. 5). Reston and McDermott (2011) suggested that such migration would result in fault abandonment as a new fault cuts up from the rift axis through the preceding footwall (Supplemental Fig. 5), and invoked this mechanism to explain unroofing of broad expanses of mantle seen in the magma-poor rifted margins between Iberia and Newfoundland. Capture of a portion of a previously rotated footwall section by a second, successor fault in this way can increase the net rotation experienced by the initial footwall, providing a mechanism capable of easily accommodating the magnitude of early rotation seen in the Mersin ophiolite.

5.2. Mode of formation and rotation of the metamorphic sole

The later, post-magmatic net rotation affecting the metamorphic sole of the Mersin ophiolite may have occurred: (i) in an intraoceanic, pre-obduction setting; (ii) during emplacement onto the Tauride margin; or (iii) have a composite origin. However, the consistency of rotation axes throughout the ophiolite is most simply explained by a common tectonic process related to spreading.

Dykes cutting the sole have geochemical signatures indicating derivation from partial melting of a depleted mantle wedge (Dilek et al., 1999). Hence the metamorphic sole must have been above this melt source during dyke intrusion, requiring a mechanism for exhuming sole rocks from peak metamorphic depths to near the top of the mantle wedge. Models for the formation of metamorphic soles involving intraoceanic thrusting of young, hot oceanic lithosphere (e.g. Çelik, 2008) require dykes to intrude through the complete footwall of the under-thrust lithosphere in order to be emplaced into the metamorphic sole along the footwall-hanging wall contact. However, an alternative model involving formation of metamorphic soles along the upper interface of a down-going plate following subduction initiation and subsequent exhumation and welding of the sole rocks to the base of overriding plate has recently been proposed by van Hinsbergen et al. (2015). This model provides a mechanism for rapid exhumation a newly-formed metamorphic sole to a position at the top of the mantle wedge, allowing post-metamorphic dyke intrusion through the sole very shortly after its formation. This is required in the case of the Tauride ophiolites, where ages of dykes and metamorphic sole rocks typically differ in age by <3 Myr (Table 1; Parlak and Delaloye, 1996, 1999; Dilek et al., 1999). The van Hinsbergen et al. (2015) model involves slab flattening in response to formation and extension of the suprasubduction zone crust, bringing sole rocks upwards to the base of the overriding lithosphere, followed by slab steepening in response to negative buoyancy resulting from eclogitization of the slab, leading to decoupling from the sole and influx of asthenosphere below the sole from which the intruding dykes derive.

This model provides a critical link between early rotation of the Mersin cumulates and mantle sequence dykes via fore-arc (hyper)extension involving oceanic detachment faulting and later rotation of dykes cutting the Mersin metamorphic sole. Welding of the metamorphic sole to the base of the mantle section via slab flattening would allow these rocks to be captured in the base of detachment fault footwall sections. This would allow rotation of the sole rocks around similar ridge-parallel, shallowly-plunging axes to those documented in the overlying ophiolite. As well as accounting for the similarity of rotation axes through the sampled units, this mechanism can also account for the rapid sequence of rotations required by our data, with all phases of rotation occurring over a restricted time interval of $<\sim 3$ Myr during which crustal accretion, formation of the sole and dyke emplacement occurred.

5.3. A conceptual model for rotation of an ophiolite and its metamorphic sole in a fore-arc environment

Linking the upper plate process of fore-arc hyperextension (Maffione et al., 2015) with the lower plate process of metamorphic sole formation and exhumation (van Hinsbergen et al., 2015) leads to a combined conceptual model (Fig. 7) that can elegantly explain rapid, near-synchronous rotation of crust, mantle and sole around consistent ridge-parallel axes. This involves the following sequence of events:

a) initiation of an intraoceanic subduction zone, resulting concurrently in the early stages of formation of the future metamorphic sole (along the upper interface of the down-going plate) and suprasubduction zone spreading in the fore-arc region above the mantle wedge. This initial phase of magmatic spreading generates cumulate gabbros in the new suprasubduction zone lower crust and emplacement of dykes in the lithospheric mantle below (Fig. 7a);
b) amagmatic detachment-mode suprasubduction spreading, resulting in rotation of cumulate gabbros and mantle-hosted dykes in the footwall of an oceanic detachment fault (D1; Fig. 7b);
c) lack of melt supply leads to migration of the D1 detachment towards the locus of rifting (Tucholke et al., 2008; Reston and McDermott, 2011; MacLeod et al., 2009), followed by initiation of a successor detachment (D2; Fig. 7c) that captures part of the rotated D1 footwall. Displacement on D2 then increases the rotation experienced by the cumulates and mantle-hosted dykes. At the same time, the down-going plate experiences slab flattening in response to suprasubduction zone spreading, mantle wedge volume decrease and upper plate extension, leading to shallowing of the future metamorphic sole and development of its inverted pressure-temperature gradient (van Hinsbergen et al., 2015);
d) at the plate contact, the metamorphic rocks at the top of the lower plate are welded to the base of the upper plate to form the metamorphic sole. Eclogitization of the lower plate then results in negative buoyancy and the initiation of slab pull, resulting in decoupling from the sole and steepening of the slab. Influx of asthenospheric mantle into the wedge generates melt and leads to intrusion of dykes into the emplaced metamorphic sole (Fig. 7d); and
e) further displacement on the D2 detachment results in additional rotation of the cumulate gabbros and mantle-hosted dykes and in disruption of the metamorphic sole, part of which rotates in the D2 footwall (Fig. 7e).

6. Conclusions

Net tectonic rotation analysis of paleomagnetic data from the suprasubduction Mersin ophiolite reveals large rotations around shallowly-plunging rotation axes that are consistently oriented NE–SW, parallel to the inferred orientation of the Neotethyan spreading axis. The data are best explained by combining recent concepts of detachment-mode spreading (leading to fore-arc hyperextension; Maffione et al., 2015) and the formation and exhumation of metamorphic soles (van Hinsbergen et al., 2015). Rotation of both the ophiolite and its metamorphic sole are inferred to be linked to rolling hinge rotation of detachment footwalls, as seen in oceanic core complexes in modern (ultra-)slow spreading lithosphere. This mode of spreading can also explain the absence of sheeted dyke complexes in several Upper Cretaceous Tauride ophiolites, as detachment-mode spreading characteristically results in tectonic juxtaposition of lower crustal and upper mantle rocks in detachment footwalls with upper crustal lavas in their hanging

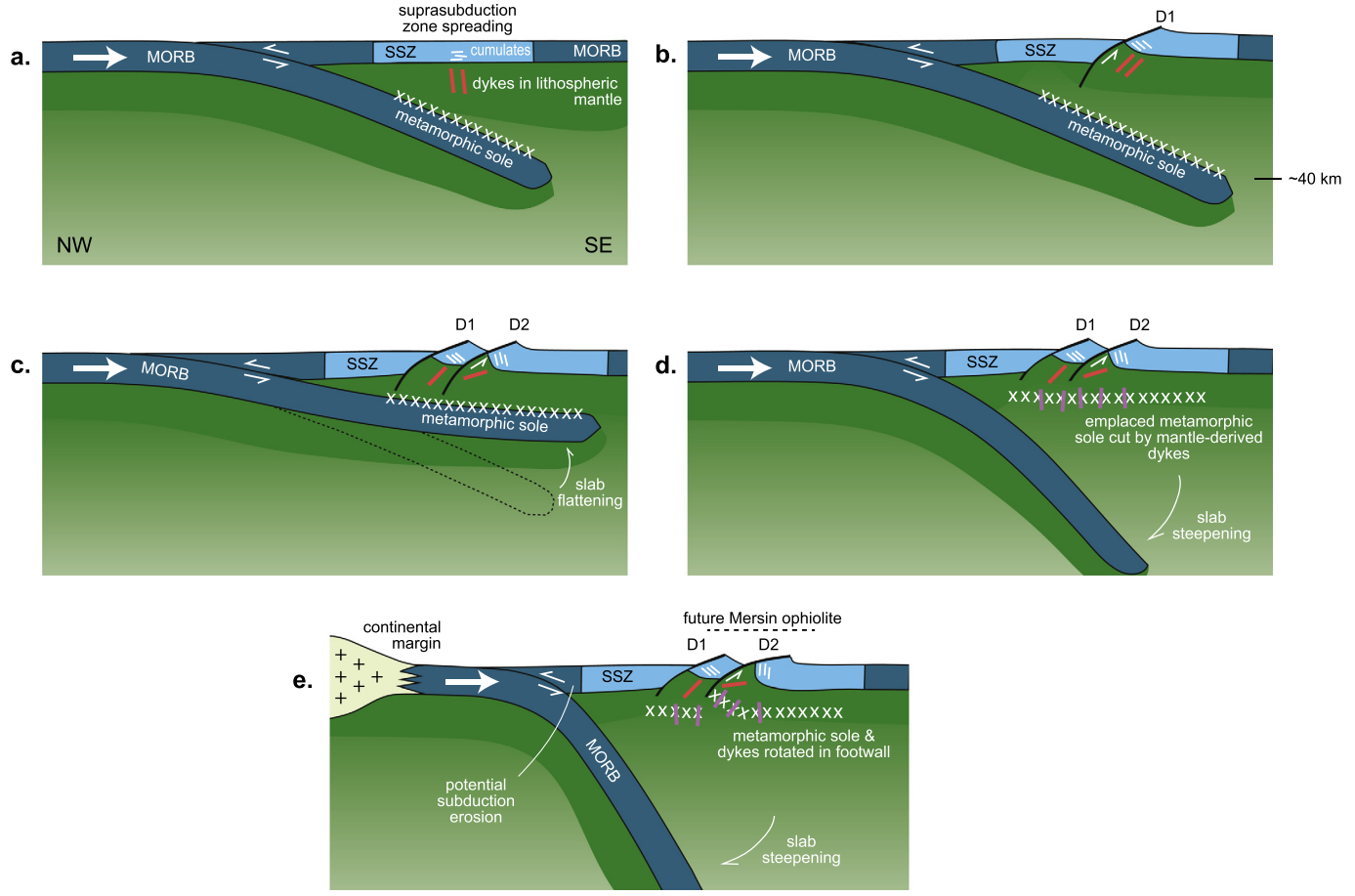

Fig. 7. Conceptual model for rapid and extreme tectonic rotation of a suprasubduction zone ophiolite and its metamorphic sole in a fore-arc environment (see text for details). Note that detachment-mode spreading in the upper plate may involve development of multiple oceanic detachment faults, but the model shows only the minimum number of structures required to explain the Mersin paleomagnetic data. (a color version of this figure is available with the web version of the article).

walls. Our results suggest that metamorphic sole rocks exhumed from peak metamorphic depths to the base of the suprasubduction zone lithosphere are then rotated as part of the upper plate. In addition, similar ages of crust and of dykes hosted in both the mantle and metamorphic sole require suprasubduction zone spreading, metamorphic sole exhumation, dyke emplacement and tectonic rotation to be essentially synchronous processes in a dynamic, intraoceanic fore-arc environment.

Acknowledgements

We thank the Ministry of Higher Education and Scientific Research (Iraq) for providing support for Ahmed Omer via a PhD scholarship held at Plymouth University. DJJvH acknowledges ERC Starting Grant 306810 (SINK) and NWO Vidi grant 864.11.004. Grateful thanks also to Osman Parlak for introducing us to the field geology of the Mersin ophiolite and for arranging field assistance by Çukurova University students during sampling. Net tectonic rotation analyses used the paleomagnetism.org application (Koymans et al., 2016). Stereographic projections and Bingham statistics were produced using Richard Allmendinger's Stereonet program v. 9.9.4 (Cardozo and Allmendinger, 2013).

Appendix A. Supplementary material

Supplementary material related to this article can be found online at http://dx.doi.org/10.1016/j.epsl.2017.08.040.

References

Allerton, S., Vine, F.J., 1987. Spreading structure of the Troodos ophiolite, Cyprus: some palaeomagnetic constraints. Geology 15, 593–597.

Cannat, M., Sauter, D., Mendel, V., Ruellan, E., Okino, K., Escartín, J., Combier, V., Baala, M., 2006. Modes of seafloor generation at a melt-poor ultraslow-spreading axis. Geology 34, 605–608. http://dx.doi.org/10.1130/G22486.1.

Cardozo, N., Allmendinger, R.W., 2013. Spherical projections with OSXStereonet. Comput. Geosci. 51, 193–205. http://dx.doi.org/10.1016/j.cageo.2012.07.021.

Çelik, Ö., 2008. Detailed geochemistry and K–Ar geochronology of the metamorphic sole rocks and their mafic dykes from the Mersin Ophiolite, Southern Turkey. Turk. J. Earth Sci. 17, 685–708.

Clube, T., Creer, K., Robertson, A., 1985. Palaeorotation of the Troodos microplate, Cyprus. Nature 317, 522–525.

Deenen, M.H.L., Langereis, C.G., van Hinsbergen, D.J.J., Biggin, A.J., 2011. Geomagnetic secular variation and the statistics of palaeomagnetic directions. Geophys. J. Int. 186, 509–520.

Dilek, Y., Thy, P., Hacker, B., Grundvig, S., 1999. Structure and petrology of Tauride ophiolites and mafic dike intrusions (Turkey): implications for the Neotethyan ocean. Geol. Soc. Am. Bull. 111, 1192.

Escartín, J., Canales, J.P., 2011. Detachments in oceanic lithosphere: deformation, magmatism, fluid flow, and ecosystems. Eos Trans. AGU 92, 31.

Garcés, M., Gee, J.S., 2007. Paleomagnetic evidence of large footwall rotations associated with low-angle faults at the Mid-Atlantic Ridge. Geology 35, 279–282.

Gee, J.S., Kent, D.V., 2007. Source of oceanic magnetic anomalies and the geomagnetic polarity time scale. In: Treatise on Geophysics, vol. 5, pp. 455–507.

Granot, R., Abelson, M., Ron, H., Lusk, M.W., Agnon, A., 2011. Direct evidence for dynamic magma supply fossilized in the lower oceanic crust of the Troodos ophiolite. Geophys. Res. Lett. 38, L16311. http://dx.doi.org/10.1029/2011GL048220.

Gurnis, M., Hall, C., Lavier, L., 2004. Evolving force balance during incipient subduction. Geochem. Geophys. Geosyst. 5, Q07001. http://dx.doi.org/10.1029/2003GC000681.

Hacker, B.R., Gnos, E., 1997. The conundrum of Samail: explaining the metamorphic history. Tectonophysics 279, 215–226.

Hurst, S.D., Verosub, K.L., Moores, E.M., 1992. Paleomagnetic constraints on the formation of the Solea graben, Troodos ophiolite, Cyprus. Tectonophysics 208, 431–445. http://dx.doi.org/10.1016/0040-1951(92)90439-D.

Inwood, J., Morris, A., Anderson, M.W., Robertson, A.H.F., 2009. Neotethyan intra-oceanic microplate rotation and variations in spreading axis orientation: palaeomagnetic evidence from the Hatay ophiolite (southern Turkey). Earth Planet. Sci. Lett. 280, 105–117.

Johnson, C.L., Constable, C.G., Tauxe, L., Barendregt, R., Brown, L.L., Coe, R.S., Layer, P., Mejia, V., Opdyke, N.D., Singer, B.S., Staudigel, H., Stone, D.B., 2008. Recent investigations of the 0–5 Ma geomagnetic field recorded by lava flows. Geochem. Geophys. Geosyst. 9, Q04032. http://dx.doi.org/10.1029/2007GC001696.

Koymans, M.R., Langereis, C.G., Pastor-Galan, D., van Hinsbergen, D.J.J., 2016. Paleomagnetism.org: an online multi-platform open source environment for paleomagnetic data analysis. Comput. Geosci. 93, 127–137.

MacDonald, W.D., 1980. Net tectonic rotation, apparent rotation, and the structural tilt correction in palaeomagnetic studies. J. Geophys. Res. 85, 3659–3669.

MacLeod, C., Allerton, S., Gass, I., Xenophontos, C., 1990. Structure of a fossil ridge–transform intersection in the Troodos ophiolite. Nature 348, 717–720.

MacLeod, C.J., Searle, R.C., Murton, B.J., Casey, J.F., Mallows, C., Unsworth, S.C., Achenbach, K.L., Harris, M., 2009. Life cycle of oceanic core complexes. Earth Planet. Sci. Lett. 287, 333–344. http://dx.doi.org/10.1016/j.epsl.2009.08.016.

MacLeod, C.J., Carlut, J., Escartín, J., Horen, H., Morris, A., 2011. Quantitative constraint on footwall rotations at the 15°45′N oceanic core complex, Mid-Atlantic Ridge: implications for detachment fault processes. Geochem. Geophys. Geosyst. 12, Q0AG03. http://dx.doi.org/10.1029/2011GC003503.

MacLeod, C.J., Dick, H.J.B., Blum, P., the Expedition 360 Scientists, 2017. Southwest Indian Ridge Lower Crust and Moho. In: Proceedings of the International Ocean Discovery Program, 360: College Station, TX (International Ocean Discovery Program). http://dx.doi.org/10.14379/iodp.proc.360.2017.

Maffione, M., Morris, A., Anderson, M.W., 2013. Recognizing detachment-mode spreading in the deep geological past. Sci. Rep. 3, 2336. http://dx.doi.org/10.1038/srep02336.

Maffione, M., van Hinsbergen, D.J.J., Koornneef, L.M.T., Guilmette, C., Hodges, K., Borneman, N., Huang, W., Ding, L., Kapp, P., 2015. Forearc hyperextension dismembered the south Tibetan ophiolites. Geology 43, 475–478. http://dx.doi.org/10.1130/G36472.1.

Maffione, M., van Hinsbergen, D., de Gelder, G., van der Goes, F., Morris, A., 2017. Kinematics of Late Cretaceous subduction initiation in the Neo-Tethys Ocean reconstructed from ophiolites of Turkey, Cyprus, and Syria. J. Geophys. Res., Solid Earth. http://dx.doi.org/10.1002/2016JB013821.

Morris, A., Anderson, M.W., 2002. Palaeomagnetic results from the Baër-Bassit ophiolite of northern Syria and their implication for fold tests in sheeted dyke terrains. Phys. Chem. Earth 27, 1215–1222.

Morris, A., Maffione, M., 2016. Is the Troodos ophiolite (Cyprus) a complete, transform fault-bounded Neotethyan ridge segment? Geology 44, 199–202. http://dx.doi.org/10.1130/G37529.1.

Morris, A., Creer, K.M., Robertson, A.H.F., 1990. Palaeomagnetic evidence for clockwise rotations related to dextral shear along the Southern Troodos Transform Fault, Cyprus. Earth Planet. Sci. Lett. 99, 250–262.

Morris, A., Anderson, M.W., Robertson, A.H.F., 1998. Multiple tectonic rotations and transform tectonism in an intra-oceanic suture zone, SW Cyprus. Tectonophysics 299, 229–253.

Morris, A., Anderson, M.W., Robertson, A.H.F., Al-Riyami, K., 2002. Extreme tectonic rotations within an eastern Mediterranean ophiolite (Baër-Bassit, Syria). Earth Planet. Sci. Lett. 202, 247–261. http://dx.doi.org/10.1016/S0012-821X(02)00782-3.

Morris, A., Gee, J.S., Pressling, N., John, B.E., MacLeod, C.J., Grimes, C.B., Searle, R.C., 2009. Footwall rotation in an oceanic core complex quantified using reorientated Integrated Ocean Drilling Program core samples. Earth Planet. Sci. Lett. 287, 217–228. http://dx.doi.org/10.1016/j.epsl.2009.08.007.

Parlak, O., Delaloye, M., 1996. Geochemistry and timing of post metamorphic dyke emplacement in the Mersin Ophiolite (southern Turkey): new age constraints from $^{40}Ar/^{39}Ar$ geochronology. Terra Nova 8, 585–592.

Parlak, O., Delaloye, M., 1999. Precise $^{40}Ar/^{39}Ar$ ages from the metamorphic sole of the Mersin ophiolite (southern Turkey). Tectonophysics 301, 145–158.

Parlak, O., Delaloye, M., Bingöl, E., 1996a. Mineral chemistry of ultramafic and mafic cumulates as an indicator of the arc-related origin of the Mersin ophiolite (southern Turkey). Geol. Rundsch. 85, 647–661.

Parlak, O., Bozkurt, E., Delaloye, M., 1996b. The obduction direction of the Mersin Ophiolite: structural evidence from subophiolitic metamorphics in the Central Tauride Belt, Southern Turkey. Int. Geol. Rev. 38, 778–786.

Parlak, O., Karaoğlan, F., Rızaoğlu, T., Klötzli, U., Koller, F., Billor, Z., 2013. U–Pb and $^{40}Ar–^{39}Ar$ geochronology of the ophiolites and granitoids from the Tauride belt: implications for the evolution of the Inner Tauride suture. J. Geodyn. 65, 22–37.

Pearce, J.A., Robinson, P.T., 2010. The Troodos ophiolitic complex probably formed in a subduction initiation, slab edge setting. Gondwana Res. 18, 60–81. http://dx.doi.org/10.1016/j.ge.2009.12.003.

Petrovský, E., Kapička, A., 2006. On determination of the Curie point from thermomagnetic curves. J. Geophys. Res. 111, 1–10.

Reston, T.J., McDermott, K.G., 2011. Successive detachment faults and mantle unroofing at magma-poor rifted margins. Geology 39, 1071–1074. http://dx.doi.org/10.1130/G32428.1.

Robertson, A.H.F., 2002. Overview of the genesis and emplacement of Mesozoic ophiolites in the Eastern Mediterranean Tethyan region. Lithos 65, 1–67.

Salisbury, M.H., Keen, C.E., 1993. Listric faults imaged in oceanic crust. Geology 21, 117–120. http://dx.doi.org/10.1130/0091-7613(1993)021<0117:LFIIOC>2.3.CO;2.

Smith, D.K., Escartín, J., Schouten, H., Cann, J.R., 2008. Fault rotation and core complex formation: significant processes in seafloor formation at slow-spreading mid-ocean ridges (Mid-Atlantic Ridge, 13°–15°N). Geochem. Geophys. Geosyst. 9, Q03003. http://dx.doi.org/10.1029/2007GC001699.

Staudigel, H., Gee, J., Tauxe, L., 1992. Shallow intrusive directions of sheeted dikes in the Troodos ophiolite: anisotropy of magnetic susceptibility and structural data. Geology 20, 841–844.

Stern, R.J., Bloomer, S.H., 1992. Subduction zone infancy: examples from he Eocene Izu-Bonin–Mariana and Jurassic California arcs. Geol. Soc. Am. Bull. 104, 1621–1636.

Tekin, U.K., Bedi, Y., Okuyucu, C., Göncüoglu, M.C., Sayit, K., 2016. Radiolarian biochronology of upper Anisian to upper Ladinian (Middle Triassic) blocks and tectonic slices of volcano-sedimentary successions in the Mersin Mélange, southern Turkey: new insights for the evolution of Neotethys. J. Afr. Earth Sci. 124, 409–426. http://dx.doi.org/10.1016/j.jafrearsci.2016.09.039.

Torsvik, T.H., Van der Voo, R., Preeden, U., Mac Niocaill, C., Steinberger, B., Doubrovine, P.V., van Hinsbergen, D.J., Domeier, M., Gaina, C., Tohver, E., 2012. Phanerozoic polar wander, palaeogeography and dynamics. Earth-Sci. Rev. 114, 325–368. http://dx.doi.org/10.1016/j.earscirev.2012.06.002.

Tucholke, B.E., Behn, M.D., Buck, W.R., Lin, J., 2008. Role of melt supply in oceanic detachment faulting and formation of megamullions. Geology 36, 455–458. http://dx.doi.org/10.1130/G24639A.1.

van Hinsbergen, D.J.J., Peters, K., Maffione, M., Spakman, W., Guilmette, C., Thieulot, C., Plümper, O., Gürer, D., Brouwer, F.M., Aldanmaz, E., Kaymakcı, N., 2015. Dynamics of intraoceanic subduction initiation: 2. Suprasubduction zone ophiolite formation and metamorphic sole exhumation in context of absolute plate motions. Geochem. Geophys. Geosyst. 16. http://dx.doi.org/10.1002/2015GC005745.

van Hinsbergen, D.J.J., Maffione, M., Plunder, A., Kaymakcı, N., Ganerød, M., Hendriks, B.W.H., Corfu, F., Gürer, D., de Gelder, G.I.N.O., Peters, K., McPhee, P.J., Brouwer, F.M., Advokaat, E.L., Vissers, R.L.M., 2016. Tectonic evolution and paleogeography of the Kırşehir Block and the Central Anatolian Ophiolites, Turkey. Tectonics 35, 983–1014. http://dx.doi.org/10.1002/2015TC004018.

Varga, R.J., Moores, E.M., 1985. Spreading structure of the Troodos ophiolite, Cyprus. Geology 13, 846–850. http://dx.doi.org/10.1130/0091-7613(1985)13<846:SSOTTO>2.0.CO;2.